Thermal conductivity of bulk and nanowire $Mg_2Si_xSn_{1-x}$ alloys from first principles

Wu Li,[1] L. Lindsay,[2] D. A. Broido,[3] Derek A. Stewart,[4] and Natalio Mingo[1]
[1]*LITEN, CEA-Grenoble, 17 rue des Martyrs, 38054 Grenoble Cedex 9, France*
[2]*Naval Research Laboratory, Washington, DC 20375, USA*
[3]*Department of Physics, Boston College, Chestnut Hill, Massachusetts 02467, USA*
[4]*Cornell Nanoscale Facility, Cornell University, Ithaca, New York 14853, USA*
(Received 29 August 2012; published 29 November 2012)

The lattice thermal conductivity (κ) of the thermoelectric materials, Mg_2Si, Mg_2Sn, and their alloys, are calculated for bulk and nanowires, without adjustable parameters. We find good agreement with bulk experimental results. For large nanowire diameters, size effects are stronger for the alloy than for the pure compounds. For example, in 200 nm diameter nanowires κ is lower than its bulk value by 30%, 20%, and 20% for $Mg_2Si_{0.6}Sn_{0.4}$, Mg_2Si, and Mg_2Sn, respectively. For nanowires less than 20 nm thick, the relative decrease surpasses 50%, and it becomes larger in the pure compounds than in the alloy. At room temperature, κ of $Mg_2Si_xSn_{1-x}$ is less sensitive to nanostructuring size effects than Si_xGe_{1-x}, but more sensitive than $PbTe_xSe_{1-x}$. This suggests that further improvement of $Mg_2Si_xSn_{1-x}$ as a nontoxic thermoelectric may be possible.

DOI: 10.1103/PhysRevB.86.174307 PACS number(s): 66.70.Df, 63.22.Gh, 63.20.dk, 84.60.Rb

I. INTRODUCTION

In the last decade, nanostructuring has proven to be a successful way to improve materials' thermoelectric figures of merit (ZT).[1,2] In most cases, enhancements in ZT result from reducing the lattice thermal conductivity. In particular, semiconductor alloys (or solid solutions) can be considerably improved, because the mean-free paths of the main heat-carrying phonons in these systems are typically much longer than the electronic mean-free paths. Empirically, it is typically easier to turn a mediocre bulk thermoelectric into a reasonably good nanostructured thermoelectric, but it is difficult to improve an already good bulk thermoelectric. Since many leading thermoelectrics rely on toxic or expensive elements, improving the ZT of cheaper and less toxic compounds could lead to cost-effective and environmentally friendly alternatives.

Since the early investigations of Ioffe,[3] the best known thermoelectric material for medium temperature(800 K) applications, such as car exhaust energy harvesting, is highly toxic lead telluride (PbTe). In recent times, $Mg_2Si_xSn_{1-x}$ alloys have emerged as a possible alternative to PbTe for medium temperature applications.[4,5] A key question is whether $Mg_2Si_xSn_{1-x}$ can be improved by nanostructuring, and by how much. $Mg_2Si_xSn_{1-x}$ alloys have a κ more than 4 times lower than the pure phases. If the low κ of alloys is due to disorder only, rather than due to grain boundaries or other natural nanostructure effects, then engineered nanostructuring could result in even lower conductivities. A previous empirical model has predicted important nanostructuring effects through nanoinclusions, but it assumed that the intrinsic conductivity of the alloy was only limited by disorder.[6] To reliably determine the role played by extrinsic scattering mechanisms in $Mg_2Si_xSn_{1-x}$ alloys, it is important to have an accurate microscopic treatment of the intrinsic κ due to phonon-phonon scattering. In this paper we rigorously determine κ of Mg_2Si, Mg_2Sn, and their alloys from first principles, as limited by phonon-phonon, isotopic impurity, and alloy scattering. We find κ for these systems in good agreement with experimental measurements. We also examine the role of boundary scattering in nanowires of Mg_2Si, Mg_2Sn, and their alloys. We show that, at room temperature, the κ of nanowires made of these materials can be reduced by half for nanowires of small diameter $\sim$20 nm.

II. METHODOLOGY

We employ the linearized Boltzmann transport equation for phonons (BTE) to examine κ for both bulk systems and nanostructures. The second-order and the third-order interatomic force constants (IFCs), which determine the phonon dispersions and scattering properties, are obtained from *ab initio* density functional theory calculations.

A. BTE

At thermal equilibrium in the absence of a temperature gradient, the phonon distribution obeys the Bose-Einstein distribution function $f_0(\omega_\lambda)$, where for each phonon mode we use the shorthand $\lambda \equiv (p,\mathbf{q})$, where p is the branch index and $\mathbf{q}$ is the wave vector. In the presence of a temperature gradient ∇T, the steady-state phonon distribution function, f_λ, can be obtained from the BTE,[7,8]

$$\nabla T \cdot \mathbf{v}_\lambda \frac{\partial f_\lambda}{\partial T} = \left.\frac{\partial f_\lambda}{\partial t}\right|_{\text{scatt}}. \quad (1)$$

The left-hand side of the equation is a diffusion term due to a temperature gradient, and the right-hand side is determined by the specific scattering events occurring in the system, such as anharmonic scattering due to phonon-phonon interactions and harmonic scattering due to impurities and defects. For a small temperature gradient, Eq. (1) can be linearized in ∇T so that $f_\lambda = f_0(\omega_\lambda) + g_\lambda$, where g_λ linearly depends on ∇T. It is convenient to write g_λ in terms of phonon lifetimes τ_λ as $g_\lambda = -\frac{dT}{dz} v^z{}_\lambda \frac{df_0}{dT} \tau_\lambda$, where we take the temperature gradient along the z direction. The BTE can then be written as[9–14]

$$\tau_\lambda = \tau^0_\lambda (1 + \Delta_\lambda), \quad (2)$$

where

$$\Delta_\lambda \equiv \frac{1}{N}\sum_{\lambda' p''}^{+}\Gamma^{+}_{\lambda\lambda'\lambda''}(\xi_{\lambda\lambda''}\tau_{\lambda''}-\xi_{\lambda\lambda'}\tau_{\lambda'}) + \frac{1}{N}\sum_{\lambda' p''}^{-}\frac{1}{2}\Gamma^{-}_{\lambda\lambda'\lambda''}(\xi_{\lambda\lambda''}\tau_{\lambda''}+\xi_{\lambda\lambda'}\tau_{\lambda'}) + \frac{1}{N}\sum_{\lambda'}\Gamma_{\lambda\lambda'}\xi_{\lambda\lambda'}\tau_{\lambda'},$$

$$1/\tau^0_\lambda \equiv \frac{1}{N}\left(\sum_{\lambda' p''}^{+}\Gamma^{+}_{\lambda\lambda'\lambda''}+\sum_{\lambda' p''}^{-}\frac{1}{2}\Gamma^{-}_{\lambda\lambda'\lambda''}+\sum_{\lambda'}\Gamma_{\lambda\lambda'}\right), \quad (3)$$

where N is the number of $\mathbf{q}$ sampling in the Brillouin zone, $\xi_{\lambda\lambda'} \equiv \omega_{\lambda'}v^z_{\lambda'}/\omega_\lambda v^z_\lambda$. In the summation $\sum^{\pm}$, $\lambda'' = (p'', \mathbf{q} \pm \mathbf{q}' + \mathbf{K})$, and $\mathbf{K}$ is a reciprocal lattice vector, which is zero for momentum-conserving normal processes and nonzero for resistive umklapp processes. The three-phonon scattering rates $\Gamma^{\pm}_{\lambda\lambda'\lambda''}$ can be expressed as

$$\Gamma^{\pm}_{\lambda\lambda'\lambda''} = \frac{\hbar\pi}{4}\begin{Bmatrix} f'_0 - f''_0 \\ f'_0 + f''_0 + 1\end{Bmatrix}\frac{\delta(\omega_\lambda \pm \omega_{\lambda'} - \omega_{\lambda''})}{\omega_\lambda\omega_{\lambda'}\omega_{\lambda''}}|V^{\pm}_{\lambda\lambda'\lambda''}|^2, \quad (4)$$

where for simplicity $f'_0 \equiv f_0(\omega_{\lambda'})$, etc., and the upper (lower) row in curly brackets goes with the $+$ $(-)$ sign, and the δ function ensures the conservation of energy. The scattering matrix elements $V^{\pm}_{\lambda\lambda'\lambda''}$ are given by[13,14]

$$V^{\pm}_{\lambda\lambda'\lambda''} = \sum_{i\in u.c.}\sum_{j,k}\sum_{\alpha\beta\gamma}\Phi^{\alpha\beta\gamma}_{ijk}\frac{e^\alpha_\lambda(i)e^\beta_{p',\pm\mathbf{q}'}(j)e^\gamma_{p'',-\mathbf{q}''}(k)}{\sqrt{M_i M_j M_k}} \quad (5)$$

and depend on the eigenfunctions of the three phonons involved, and the third-order interatomic force constants $\Phi^{\alpha\beta\gamma}_{ijk} = \frac{\partial^3 E}{\partial r^\alpha_i \partial r^\beta_j \partial r^\gamma_k}$. The atomic indices are given by i, j, and k and the Cartesian components by α, β, and γ. In the sums, i runs through just one unit cell, which we shall call the central unit cell; j and k run over the whole system. r^α_i and M_i are the α component of the displacement from the equilibrium position and the mass of the ith atom, respectively. $e^\alpha_\lambda(i)$ denotes the α component of the eigenfunction of mode λ at the ith atom. These eigenfunctions are normalized to 1 inside the unit cell. Generally we have $\mathbf{e}_{p,-\mathbf{q}} = \mathbf{e}^*_{p,\mathbf{q}}$.

We include an isotopic impurity scattering probability $\Gamma_{\lambda\lambda'}$ given by[12,15]

$$\Gamma_{\lambda\lambda'} = \frac{\pi\omega^2}{2}\sum_{i\in u.c.} g(i)|\mathbf{e}^*_\lambda(i)\cdot\mathbf{e}_{\lambda'}(i)|^2\delta(\omega-\omega'), \quad (6)$$

where the mass variance, $g(i)$, is given by $g(i) = \sum_s f_s(i)[1 - M_s(i)/\bar{M}(i)]^2$, with $f_s(i)$ and $M_s(i)$ being the concentration and mass of the sth isotope of atom i and $\bar{M}(i)$ is the average mass of the ith atom in the unit cell. The mass variances for Mg, Si, and Sn are 7.399×10^{-4}, 2.007×10^{-4}, and 3.341×10^{-4}, respectively. We use a virtual crystal approach to treat $Mg_2Si_xSn_{1-x}$, where the lattice constant, masses, and IFCs of the virtual crystal are taken as the average of those for the constituent materials depending on the concentration.[16] Furthermore, the disorder of IFCs is neglected, and the alloy mass disorder is included in the same way as the isotopes.

Equation (2) is solved numerically for τ_λ with an iterative approach. The zeroth-order solution $\tau^{(0)}_\lambda = \tau^0_\lambda$, which neglects Δ_λ, is equivalent to the relaxation time approximation (RTA). This iterative procedure is important for materials such as diamond where a significant portion of the phonon-phonon scattering events are due to normal processes. However, in materials such as silicon and germanium with strong umklapp scattering, the iterative procedure leads to less than a 10% increase in the room temperature thermal conductivity compared to the RTA result.[13] For Mg_2Si, Mg_2Sn, and the alloys studied in this paper, we also find the iteration is not important; for instance, the differences are 1.7% and 0.5% for Mg_2Si and Mg_2Sn, respectively, at 300 K.

With τ_λ determined, the heat flux can be calculated, and κ obtained as

$$\kappa = \frac{1}{NVk_BT^2}\sum_\lambda f_0(f_0+1)(\hbar\omega_\lambda)^2\left(v^z_\lambda\right)^2\tau_\lambda, \quad (7)$$

where V is the volume of the unit cell. The bulk κ is a scalar, for the cubic structures considered here. In nanostructures such as nanowires, the phonon lifetimes are position dependent due to the presence of the nanowire walls. For this case, the BTE has an additional space-dependent term

$$1 = \left(\tau^0_\lambda\right)^{-1}\tau_{\mathbf{r},\ \lambda} - \Delta_{\mathbf{r},\ \lambda} + \mathbf{v}_\lambda\cdot\nabla\tau_{\mathbf{r},\lambda}, \quad (8)$$

where the dependence of $\Delta_{\mathbf{r},\lambda}$ on $\tau_{\mathbf{r},\lambda}$ is the same as that for Δ_λ on τ_λ. Previously we have presented an approximate iterative solution to Eq. (8).[17] Since for $Mg_2Si_xSn_{1-x}$, $\Delta_{\mathbf{r},\lambda}$ can be neglected, one has the formal solution[8]

$$\tau_{\mathbf{r},\lambda} = \tau^0_\lambda\left[1-\exp\left(-\left|\frac{\mathbf{r}-\mathbf{r}_b}{\tau^0 v_\lambda}\right|\right)G_{\mathbf{r},\lambda}\right], \quad (9)$$

where $\mathbf{r}_b$ is a point on the surface of the nanowire where a phonon in mode λ can reach moving backwards from $\mathbf{r}$, and $G_{\mathbf{r},\lambda}$ is determined by the boundary conditions. For completely diffusive boundary scattering, as considered here, $G_{\mathbf{r},\lambda} = 1$. The average of $\tau_{\mathbf{r},\lambda}$ over the cross section, $\bar{\tau}_\lambda$, can thus be obtained as

$$\bar{\tau}_\lambda = \tau^0_\lambda\left\{\frac{1}{S_c}\int_{S_c}\left[1-\exp\left(-\left|\frac{\mathbf{r}-\mathbf{r}_b}{\tau^0 v_\lambda}\right|\right)\right]d\mathbf{s}\right\}, \quad (10)$$

with S_c being the nanowire cross section. Replacing τ_λ with $\bar{\tau}_\lambda$ in Eq. (7) determines the nanowire thermal conductivity.

B. *Ab initio* calculation of IFCs

Both the second- and third-order IFCs can be calculated by using either density functional perturbation theory (DFPT)[13,18,19] or a real-space finite difference supercell approach within density functional theory (DFT).[20,21] DFPT is a linear response approach which uses a reciprocal space representation. Since phonons are, by definition, commensurate with the crystal lattice, they can be defined in terms of q vectors in the first Brillouin zone. This makes the DFPT approach computationally efficient,[18] because both electronic structure and phonon calculations can be done within the first Brillouin zone. Since Mg_2Si and Mg_2Sn are polar materials, an additional linear response calculation of the Born effective

charge and dielectric tensor is required to determine the nonanalytic part of the dynamical matrix at the Γ point which leads to the LO-TO splitting. For comparison, we calculate the second-order IFCs using both methods. The phonon frequencies, velocities, and eigenvectors are then obtained by diagonalizing the dynamical matrix. While harmonic force constants can be obtained with DFPT in standard plane wave packages such as QUANTUM ESPRESSO, the ability to calculate anharmonic IFCs is not available in widely distributed codes. To determine the third-order IFCs, we use a real-space finite difference method:

$$\begin{aligned}\Phi_{ijk}^{\alpha\beta\gamma} &= \frac{\partial^3 E}{\partial r_i^\alpha \partial r_j^\beta \partial r_k^\gamma} \\ &= \left[\frac{\partial^2 E}{\partial r_j^\beta \partial r_k^\gamma}\left(r_i^\alpha = h\right) - \frac{\partial^2 E}{\partial r_j^\beta \partial r_k^\gamma}\left(r_i^\alpha = -h\right)\right] \Big/ 2h \\ &= \frac{1}{4h^2}\left[F_k^\gamma\begin{pmatrix} r_i^\alpha = h \\ r_j^\beta = -h\end{pmatrix} - F_k^\gamma\left(r_i^\alpha = h r_j^\beta = h\right)\right. \\ &\quad \left. + F_k^\gamma\begin{pmatrix} r_i^\alpha = -h \\ r_j^\beta = h\end{pmatrix} - F_k^\gamma\begin{pmatrix} r_i^\alpha = -h \\ r_j^\beta = -h\end{pmatrix}\right], \end{aligned} \tag{11}$$

where h is a small displacement from the equilibrium position, and F_k^γ is the γ component of the force felt by the kth atom. Not all of the force constant elements are independent of each other. $\Phi_{ijk}^{\alpha\beta\gamma}$ should satisfy the permutation symmetry and the space group symmetry of the system. Consider a general space group symmetry operation $\sum_\alpha T^{\alpha'\alpha} R_i^\alpha + b^{\alpha'} = R_{Tb(i)}^{\alpha'}$, where T and $\mathbf{b}$ stand for the point group operator and translation operator, respectively, and Tb(i) specifies the atom to which the ith atom is mapped under the corresponding operation. The third-order IFCs tensor should satisfy the following relation:

$$\Phi_{Tb(i);Tb(j);Tb(k)}^{\alpha'\beta'\gamma'} = \sum_{\alpha\beta\gamma} T^{\alpha'\alpha} T^{\beta'\beta} T^{\gamma'\gamma} \Phi_{ijk}^{\alpha\beta\gamma}. \tag{12}$$

Mg_2Si and Mg_2Sn belong to the space group $Fm\bar{3}m$, for which all the elements of $T^{\alpha'\alpha}$ are integers. Therefore, the dependence of the IFC elements is relatively simple, one element being related to another by plus, minus, or zero. If an element is the opposite of itself, it should vanish.

For practical purposes, a cutoff radius is defined such that atoms farther than the cutoff are considered noninteracting. Here, we choose a cutoff radius of $0.85a$, where a is the lattice constant, that is, up to fourth-nearest neighbors are included for Mg, and up to third-nearest neighbors are included for Si or Sn. We have previously tested the effects of nearest-neighbor cutoff radius for Si, Ge, GaAs, and GaP, and find κ insensitive to the inclusion of more interactions. Application of symmetries dramatically reduces the number of independent IFCs that must be determined. Within this cutoff radius, there are 233 nonzero independent anharmonic elements to be calculated out of a total of 57 753 elements. Due to this truncation, the calculated IFCs do not exactly satisfy the sum rules required by translational invariance. This invariance plays a critical role in determining the zone-center phonon-phonon scattering rates and is thus enforced via different approaches, which will be addressed in the next section.

C. Enforcement of the third-order IFC sum rules

Due to the fact that the system energy does not change if the system as a whole is displaced, we have the sum rules for third-order IFCs

$$\sum_k \Phi_{ijk}^{\alpha\beta\gamma} = 0. \tag{13}$$

This equation is still valid if the summation is over i or j due to the permutation symmetry.

The directly calculated force constants from any *ab initio* package do not exactly satisfy all the sum rules, though the sums in Eq. (13) are typically small if not zero. Since these sum rules are crucial to obtain the correct scattering rates at low frequencies, they have to be enforced by changing the original calculated force constants slightly. There are different methods to do so. For example, a small set of anharmonic IFCs for interactions only within the unit cell can be changed to satisfy the sum rules similar to the typical "acoustic sum rule" applied to the second-order IFCs in standard DFPT packages. However, this violates other system symmetries. The translational invariance conditions can also be satisfied by a minimization of the sum of the square of the sums given in Eq. (13) in a high-dimensional parameter space. This results in the enforcement of the sum rule while maintaining permutation and point group symmetries. It can also be done by solving an optimization problem. The idea of the latter method is to add a compensation d_i to each independent nonzero element ϕ_i, where i ranges from 1 to the total number of independent nonzero elements, such that the sum rule condition can be satisfied. In order to guarantee that the compensation is small, some additional constraints need to be considered. Here we minimize the sum of the squares of the compensation for each independent nonzero element. This is not the only choice; for instance, the sum of the squares of the compensations for all the dependent nonzero elements could be minimized. We use here the former case, and the enforcement of sum rules turns out to be a minimization of a quadratic polynomial subject to constraints, which can be easily done by using the Lagrange multipliers method. In previous work, we have used a similar Lagrange multiplier technique to symmetrize first-principles harmonic force constants.[22]

The sums are not linearly independent, and the independent sums can be found numerically. Since all the force constants can be deduced from the independent elements, the sums can be written in terms of these elements as

$$\sum_j A_{ij}\phi_j = B_i, \tag{14}$$

where A_{ij} are integers in the case of a cubic system, and j ranges from 1 to the total number of independent sums. Since the sum rules have to be satisfied, the constraints on the compensation are

$$g_i \equiv \sum_j A_{ij} d_j + B_i = 0. \tag{15}$$

The function to be minimized is

$$f = \frac{1}{2}\sum_j d_j^2. \tag{16}$$

After introducing the Lagrange multiplier λ_i, the expression of d_j in terms of λ_i is obtained from

$$\frac{\partial(f+\sum_i \lambda_i g_i)}{\partial d_j} = 0, \tag{17}$$

from which it follows

$$d_j = -\sum_i \lambda_i A_{ij}. \tag{18}$$

Substituting this relation into Eq. (15), we have

$$\sum_j C_{ij}\lambda_j = B_i, \tag{19}$$

with $C_{ij} = \sum_m A_{im}A_{jm}$. λ_j can be obtained by solving the linear equation arrays, and d_j is further obtained by using Eq. (18). When d_j is added to the independent IFC elements, ϕ_j, the sum rules are completely satisfied and the compensations are minimized. Different methods lead to similiar results.

III. RESULTS AND DISCUSSION

We calculated the *ab initio* harmonic IFCs, Born effective charges, and dielectric tensor based on DFPT using the QUANTUM ESPRESSO package.[23] For comparison, we also used the SIESTA package[24] to calculate harmonic IFCs based on the supercell approach. The local density approximation (LDA) was used to describe the electron exchange and correlation energy in both cases. The anharmonic IFCs were calculated using both packages separately and based on the supercell technique. QUANTUM ESPRESSO uses a plane wave basis set while SIESTA uses a numerically truncated localized basis set, which enables faster calculation.

A. Phonon dispersions

Preceding all IFC calculations, structural relaxations were performed to determine the minimum energy unit cell for both Mg_2Si and Mg_2Sn. A 24×24×24 Monkhorst-Pack k-point mesh was used to sample the Brillouin zone in the electronic structure calculations to determine the self-consistent charge density and potential. For the QUANTUM ESPRESSO calculations, a plane wave cutoff of 80 Ry and an 800 Ry energy cutoff was used for the charge density and potential. A von Barth–Car norm-conserving pseudopotential[25] was used to describe silicon and Bachelet-Hamann-Schlüter pseudopotentials[26] were used to describe magnesium and tin. Phonon calculations based on DFPT sampled the interatomic force constants on an 8 × 8 × 8 Monkhorst-Pack q-point mesh which were then interpolated to determine the full phonon dispersion. In the case of the real-space SIESTA calculations, we used a double zeta polarized basis set to describe the localized orbitals in all calculations. A mesh cutoff of 400 Ry was used to avoid egg-box effects which can cause errors in the calculated forces.[24] In the case of Mg_2Sn, as discussed below, we also found that grid cell sampling[24] was required for accurate phonon dispersions. For both Mg_2Si and Mg_2Sn, a 5 × 5 × 5 supercell with a 4 × 4 × 4 Monkhorst-Pack k-point grid was used for real-space calculations that gave reasonable agreement with the plane wave result and experiments.

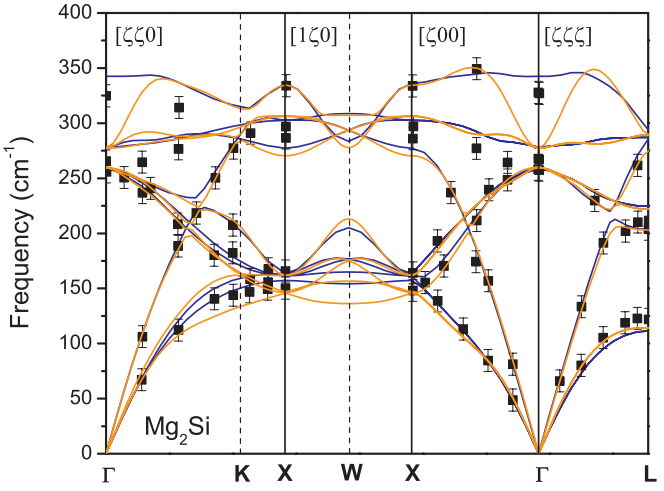

FIG. 1. (Color online) Phonon dispersion for Mg_2Si along different symmetry lines. The dispersion calculated using density functional perturbation theory with an 8 × 8 × 8 q-point grid is given by the solid blue lines. The orange lines denote the phonon dispersion calculated using the real-space force constant approach with a 5 × 5 × 5 supercell. Experimental results from Hutchings *et al.* (Ref. 31) taken at room temperature are denoted by black squares.

Given the renewed interest in Mg_2X thermoelectrics, several groups have recently calculated the phonon dispersion of these systems from first principles.[27–30] Many of these calculations use either a sparse 4 × 4 × 4 DFPT q-point mesh or a smaller supercell for real-space calculations which is sufficient for identifying general features of the phonon dispersion. However, coarser grids can lead to underestimates of the phonon velocities and difficulty predicting the flat dispersions in the transverse acoustic branches near the X and L symmetry points. An accurate phonon dispersion is critical for determining the phonon velocities and phonon-phonon interactions required for thermal conductivity calculations. In this work, our calculations include longer range interatomic force constants with stricter convergence criteria to better describe the phonon dispersion.

Figure 1 shows the calculated phonon dispersion using both the plane wave DFPT technique (blue curves) and the supercell approach (orange curves) for Mg_2Si with Hutchings *et al.*'s neutron diffraction results[31] (black squares). Overall, the agreement between the two approaches and experimental data is quite good. The supercell approach, which lacks the Born effective charges and dielectric tensor, does not reproduce the LO-TO splitting at the Γ point in the high-frequency optical branches. The biggest difference occurs along the Γ-K-X symmetry line where the DFPT approach does a better job of matching experiment compared to the supercell approach for the transverse acoustic branches. This may be due to the fact that the DFPT approach includes longer range interactions, effectively a 8 × 8 × 8 supercell, compared to the real-space 5 × 5 × 5 supercell calculation. It should be noted that the lower optical branches are fairly dispersive which indicates that the optical modes have a significant group velocity.

The calculated phonon dispersion of Mg_2Sn using QUANTUM ESPRESSO and SIESTA (Fig. 2) displays some interesting features which deserve a brief discussion. Mg_2Sn is

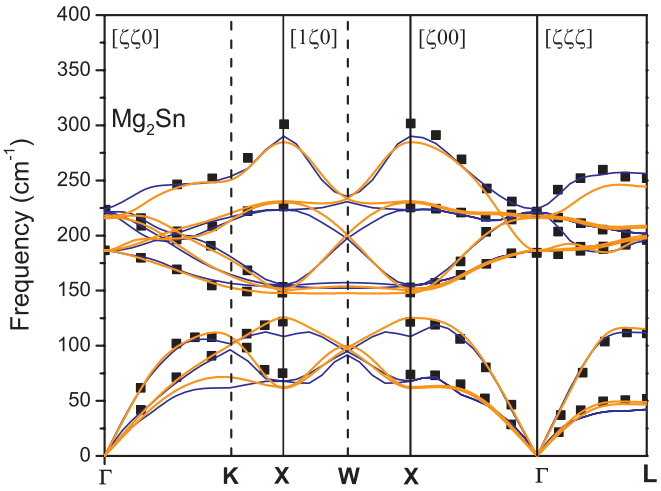

FIG. 2. (Color online) The Mg_2Sn phonon dispersion is shown along different symmetry lines. The solid blue lines denote the dispersion calculated using density functional perturbation theory with an $8 \times 8 \times 8$ q-point grid. The phonon dispersion calculated using the real-space force constant approach with a $5 \times 5 \times 5$ supercell is given by the solid orange lines. Experimental results from Kearney *et al.* (Ref. 32) taken at room temperature are denoted by black squares. Experimental errors are comparable to the size of the black squares.

a small band gap semiconductor. However, density functional theory is well known to underestimate band gaps and, in the case of Mg_2Sn, both QUANTUM ESPRESSO and SIESTA predict a semimetal with a Fermi surface containing a small hole pocket at the Γ point and small electron pocket at the X point. Recent work by another group has also noted this metallic behavior.[33] This raises the question of whether this change in electronic structure will affect the calculated phonon dispersion. However, we find that the calculated phonon dispersions using both QUANTUM ESPRESSO (DFPT) and SIESTA (real-space approach) show good agreement with the room temperature data from Kearney *et al.*[32] The LO-TO splitting at the Γ point is also well represented. While the real-space supercell calculations do a reasonably good job of reproducing the experimental phonon dispersions along the high-symmetry lines, we found that using grid cell sampling in the SIESTA calculations was essential to avoid the egg-box effect[24] and accurately predict TA acoustic branches near the X point.

B. Thermal conductivity

For the thermal conductivity calculations, only the phonon frequencies and velocities determined by the QUANTUM ESPRESSO package were used because they gave a better fit to experimental phonon dispersions in both cases. The third-order IFCs calculated by using QUANTUM ESPRESSO and SIESTA are quite close, with only around 1% difference for the larger IFC elements. Figure 3 shows the room temperature scattering rates $1/\tau_\lambda^0$ contributed by only three-phonon processes for LA modes of Mg_2Si along the Γ-K direction in the Brillouin zone calculated using these different packages. The differences of the scattering rates are quite small, especially for low frequencies, which leads to very close κ's. The low-frequency scattering rates follow the expected ω^2 dependence.[34] With

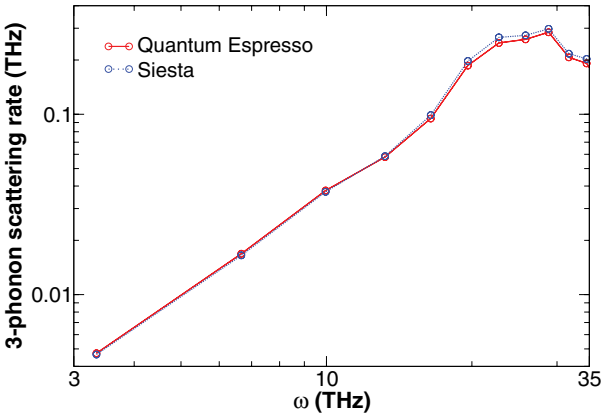

FIG. 3. (Color online) Three-phonon scattering rates for the LA branch of Mg_2Si along the Γ-L direction in the Brillouin zone calculated by using third-order IFCs obtained with the QUANTUM ESPRESSO package (solid lines) and SIESTA package (dashed lines). The low-frequency scattering rates follow well the expected ω^2 dependence.

the QUANTUM ESPRESSO third-order IFCs we calculate κ of 11.30 W/mK, while using SIESTA we calculate 10.93 W/mK at room temperature for Mg_2Si. In the latter part of the paper, the presented calculation results were obtained by using the QUANTUM ESPRESSO IFCs.

Phonon-isotope scattering can play an important role in determining κ.[35,36] Including naturally occurring isotope concentrations we find that the room temperature κ is reduced by 10% and 4% in Mg_2Si and Mg_2Sn, respectively, compared with the isotopically pure compounds. The isotope effect is mainly due to Mg isotopes, which has a larger mass variance than Si and Sn.

Figure 4 shows the calculated $\kappa(T)$ for Mg_2Si and Mg_2Sn with experimental values. The reported experimental values for Mg_2Si are scattered in a relatively wide range,[37–42] and

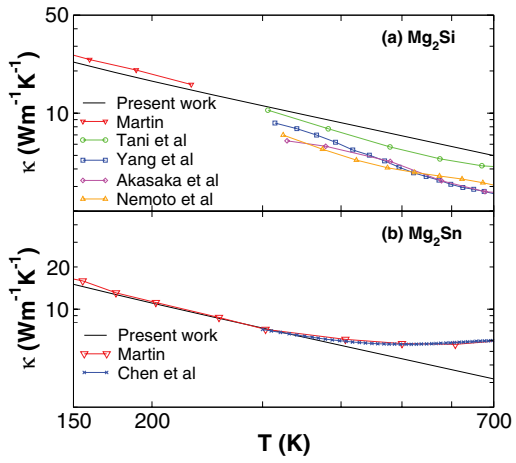

FIG. 4. (Color online) Calculated lattice κ versus temperature for (a) Mg_2Si and (b) Mg_2Sn, compared with experimental data of Martin *et al.* (Ref. 37), Tani *et al.* (Ref. 38), Yang *et al.* (Ref. 39), Akasaka *et al.* (Ref. 40), Nemoto *et al.* (Ref. 41), and Chen *et al.* (Ref. 42). Data of Martin *et al.* are the total thermal conductivity and the other experimental data are the extracted lattice thermal conductivity.

our calculated results lie within the range of κ's measured in experiments. Experimentally, the lattice κ were extracted from the measured total κ using the Wiedemann-Franz law. Data taken from Ref. 37 are the total thermal conductivity including the electronic contribution, which accounts for less than 4% for Mg_2Sn at room temperature.[42] Due to the neglect of the bipolar contribution to the electronic thermal conductivity, there is a spurious increase at high temperatures in the extracted lattice κ in Ref. 42. The calculated results roughly scale inversely with temperature, similar to the experimental data. It has been previously reported that using fully relativistic pseudopotentials, including spin-orbital interactions, could lead to calculated κ's for PbSe and PbTe that are two times larger than those obtained using nonrelativistic pseudopotentials.[43] Considering the relatively small discrepancies with the experimental data obtained here, the use of fully relativistic pseudopotentials might not be important for Mg_2Si and Mg_2Sn.

It is evident in Fig. 4 that κ for Mg_2Si is larger than that for Mg_2Sn. Interestingly, we find that the phonon lifetimes of Mg_2Sn are larger than those for Mg_2Si for the same $\mathbf{q}$ points in the Brillouin zone. However, the larger group velocities in the acoustic branches of Mg_2Si play a more important role and result in it having larger κ than that in Mg_2Sn. Optical modes account for more than 30% and 18% of the total κ at room temperature for Mg_2Si and Mg_2Sn, respectively, and even more at higher temperatures, which means that the contribution of optical modes cannot be simply neglected, as is often done in many materials. Moreover, the optical modes provide important scattering channels for the heat-carrying acoustic modes as demonstrated in diamond, GaN, PbTe, PbSe, etc.[13,36,43]

It is instructive to examine the distribution of phonon mean-free paths (MFPs) in Mg_2Si, Mg_2Sn, and alloys. A clear view of the MFP distribution is provided by the normalized "cumulative thermal conductivity," κ_l/κ, which represents the fraction of heat carried by phonons with MFPs shorter or equal to l.[44] We plot the normalized cumulative thermal conductivity for Mg_2Si, Mg_2Sn, and $Mg_2Si_{0.6}Sn_{0.4}$ in Fig. 5. For the alloy case, harmonic scattering due to mass differences is increased, resulting in a reduced κ. For low-frequency phonon modes with large MFPs the anharmonic scattering dominates so the main reduction of κ with alloying comes from high-frequency modes with small MFPs. As a result, the normalized cumulative thermal conductivity of $Mg_2Si_{0.6}Sn_{0.4}$ alloy is lower than that for pure systems at large MFPs. On the other hand, there are more phonon modes with MFP smaller than a given short MFP in alloys, leading to a larger fraction of heat carried by modes with short MFPs. The curves for the pure phase and the alloy are expected to cross for the intermediate MFPs.

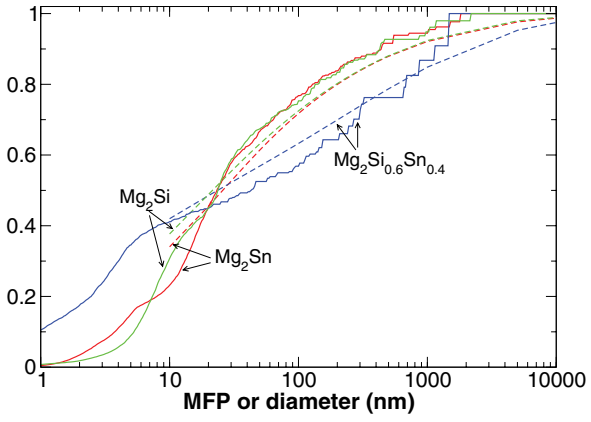

FIG. 5. (Color online) Solid lines: Normalized cumulative thermal conductivity of bulk Mg_2Si, Mg_2Sn, and $Mg_2Si_{0.6}Sn_{0.4}$ at room temperature, as a function of the mean-free path. Dashed lines: Room temperature thermal conductivities of Mg_2Si, Mg_2Sn, and $Mg_2Si_{0.6}Sn_{0.4}$ nanowires as a function of diameter, normalized by their corresponding bulk values.

The cumulative function is a useful tool for understanding the size dependence of κ in nanowires, since one expects that phonons with MFPs much longer than the boundary size will be strongly scattered by the boundary, thus limiting considerably their contribution to the conductivity. In Fig. 5 we also show κ's of Mg_2Si, Mg_2Sn, and $Mg_2Si_{0.6}Sn_{0.4}$ nanowires along the [001] growth direction normalized to their corresponding bulk values. The normalized κ's of nanowires and the cumulative thermal conductivity match reasonably well. For instance, similar to the cumulative thermal conductivity, the normalized κ's of Mg_2Si and Mg_2Sn nanowires are almost identical above 100 nm. The κ's of $Mg_2Si_{0.6}Sn_{0.4}$ nanowires show a larger percentage decrease with decreasing diameters above 20 nm than Mg_2Si and Mg_2Sn, which is reflected in the cumulative thermal conductivity. In 200 nm nanowires κ is lower than its bulk value by 30%, 20%, and 20% for $Mg_2Si_{0.6}Sn_{0.4}$, Mg_2Si, and Mg_2Sn, respectively. The cumulative thermal conductivity picture also suggests a 50% reduction of the κ's of nanowires at 20 nm for all three systems, which is confirmed by the actual calculation. For nanowires less than 20 nm thick, the relative decrease surpasses 50%, and it becomes larger in the pure compounds than in the alloy, since there is less heat carried by phonons with MFPs larger than 20 nm in the alloy.

The diameter at which κ is reduced by half is quite different from material to material. It is 5 nm, 20 nm, and larger than 200 nm for $PbSe_xTe_{1-x}$, $Mg_2Si_xSn_{1-x}$, and Si_xGe_{1-x}, respectively,[17,43] at room temperature, which means that κ of $Mg_2Si_xSn_{1-x}$ is less sensitive to nanostructuring size effects than Si_xGe_{1-x}, but more sensitive than $PbTe_xSe_{1-x}$. Actually the bulk κ's of these materials increase in the same order, and the relation between the thermal conductivity and the degree of difficulty to reduce the thermal conductivity in nanostructures is not a coincidence. Larger thermal conductivity arises typically because of weaker intrinsic phonon-phonon scattering, which causes phonons to have larger MFPs, and these can be more easily blocked by boundaries of a similar size. Therefore the lower the intrinsic thermal conductivity, the harder it is to reduce it further in nanostructures. This can serve as an empirical guide for engineering thermal transport in nanostructures.

The calculated room temperature κ's of $Mg_2Si_xSn_{1-x}$ as a function of x are plotted in Fig. 6 for both bulk materials and 20 nm nanowires. Experimental values for bulk alloys are also plotted.[4,5,38,42] The agreement with experiments is reasonably good at the intermediate concentrations. The theory obtains a minimum κ of 2.07 W/K-m, which is close to the experimental minimum 1.89 W/K-m. A small amount of alloying can reduce κ's of pure compounds significantly, and such behavior

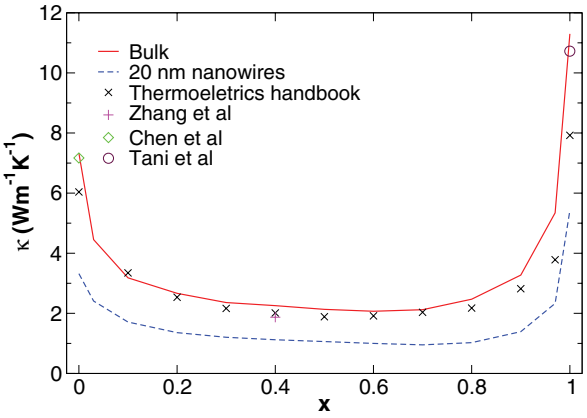

FIG. 6. (Color online) Room temperature κ of $Mg_2Si_xSn_{1-x}$ as a function of x for both bulk materials (solid line) and 20 nm nanowires along [001] growth direction (dashed line), compared with experimental data taken from the *Thermoelectrics Handbook* (Ref. 4), Zhang *et al.* (Ref. 5), Chen *et al.* (Ref. 42), and Tani *et al.* (Ref. 38).

was observed in many materials.[16,43,45–47] In nanowires, the reduction of κ with alloying is not as strong as in bulk systems because boundary scattering plays a significant role, relatively weakening the mass difference scattering.[48–50] In nanowires of $Mg_2Si_xSn_{1-x}$, the x value at which κ is minimized is slightly different from that for the bulk systems shifting from 0.6 for bulk to 0.7 for 20 nm nanowires. At higher temperature, the anharmonic scattering becomes stronger and weakens the role played by the alloy scattering as well, and therefore $\kappa(x)$ becomes smoother, similarly to the case for the nanowires.

Reference 5 found that κ of alloy $Mg_2Si_xSn_{1-x}$ can be further decreased by doping with Sb, and suggested that the decrease is due to intrinsic nanodots rather than the enhanced mass difference. We consider further doping $Mg_2Si_{0.3925}Sn_{0.6}Sb_{0.0075}$. Since the concentration of Sb is not large, we neglect the possible changes in the IFCs and treat the doping of Sb as a simple mass difference scattering. The calculated κ is decreased by only 1%, confirming that the mass difference is not the only mechanism for the effect of doping upon κ observed in Ref. 5. The nondoped material's room temperature κ reported in Ref. 5 was 1.87 W/m-K, within 18% of our calculated value 2.26 W/m-K. This implies that even if there was some natural nanostructuring (i.e., naturally occurring nanoinclusions) in the undoped samples, purposely nanostructuring in $Mg_2Si_xSn_{1-x}$, via nanowires or added nanoinclusions, can still decrease the thermal conductivity of the compounds by a meaningful amount.

IV. CONCLUSION

We have calculated the κ of $Mg_2Si_xSn_{1-x}$ alloys and pure phases via a microscopic, *ab initio* Boltzmann transport approach without fitting parameters. Given an accurate treatment of intrinsic anharmonic phonon scattering, we have evaluated the thermal conductivity reduction in these compounds due to nanostructure size effects, focusing in particular on nanowires. We find the relative decrease of κ in these compounds and alloys due to nanostructuring to be less than in Si, Ge, and Si_xGe_{1-x}, but more than in PbTe, PbSe, and $PbTe_xSe_{1-x}$. In nanowires below a characteristic size of 20 nm thickness, the pure phases begin to display larger reductions than the alloy. At that typical size, κ for all cases is shown to decrease to about half its bulk value at room temperature. This suggests that $Mg_2Si_xSn_{1-x}$ may still benefit from nanostructuring in order to achieve its full potential as a thermoelectric material. Accurate, predictive determination of intrinsic phonon-phonon scattering through this *ab initio* method will allow for more reliable predictions of the role of nanostructuring on ZT in other thermoelectric compounds.

ACKNOWLEDGMENTS

We acknowledge support from Agence Nationale de la Recherche through project ACCATTONE and CEA through project THERMA and the EU project NEAT. L.L. acknowledges support from DARPA, the NRC/NRL Research Associateship Program, and the XSEDE program, which is supported by NSF Grant No. OCI-1053575. D.A.B. acknowledges support from the National Science Foundation under Grant No. 1066634 and from the S3TEC, an Energy Frontier Research Center funded by the US Department of Energy, Office of Science, Office of Basic Energy Sciences, under Award No. DE-FG02-09ER46577. D.A.S. acknowledges support from the NSF under Grant No. 1066406. A portion of the calculations for this work were performed on the Intel Cluster at the Cornell Nanoscale Facility, part of the National Nanotechnology Infrastructure Network (NNIN), funded by the NSF.

[1] A. I. Hochbaum, R. Chen, R. D. Delgado, W. Liang, E. C. Garnett, M. Najarian, A. Majumdar, and P. Yang, Nature (London) **451**, 163 (2008).
[2] C. J. Vineis, A. Shakouri, A. Majumdar, and M. Kanatzidis, Adv. Mater. **22**, 3970 (2010).
[3] A. F. Ioffe, *Semiconductor Thermoelements and Thermoelectric Cooling* (Infosearch, London, 1957).
[4] D. M. Rowe, *Thermoelectrics Handbook* (Taylor & Francis, 2005).
[5] Q. Zhang, J. He, T. J. Zhu, S. N. Zhang, X. B. Zhao, and T. M. Tritt, Appl. Phys. Lett. **93**, 102109 (2008).
[6] S. Wang and N. Mingo, Appl. Phys. Lett. **94**, 203109 (2009).
[7] R. E. Peierls, *Quantum Theory of Solids* (Oxford University Press, London, 1955).
[8] J. M. Ziman, *Electrons and Phonons* (Clarendon Press, 1962).
[9] M. Omini and A. Sparavigna, Phys. Rev. B **53**, 9064 (1996).
[10] M. Omini and A. Sparavigna, Nuovo Cimento D **19**, 1537 (1997).
[11] D. A. Broido, M. Malorny, G. Birner, N. Mingo, and D. A. Stewart, Appl. Phys. Lett. **91**, 231922 (2007).
[12] A. Kundu, N. Mingo, D. A. Broido, and D. A. Stewart, Phys. Rev. B **84**, 125426 (2011).
[13] A. Ward, D. A. Broido, D. A. Stewart, and G. Deinzer, Phys. Rev. B **80**, 125203 (2009).

[14]L. Lindsay, D. A. Broido, and N. Mingo, Phys. Rev. B **82**, 161402(R) (2010).
[15]S.-i. Tamura, Phys. Rev. B **27**, 858 (1983).
[16]B. Abeles, Phys. Rev. **131**, 1906 (1963).
[17]W. Li, N. Mingo, L. Lindsay, D. A. Broido, D. A. Stewart, and N. A. Katcho, Phys. Rev. B **85**, 195436 (2012).
[18]S. Baroni, S. de Gironcoli, A. D. Corso, and P. Giannozzi, Rev. Mod. Phys. **73**, 515 (2001).
[19]G. Deinzer, G. Birner, and D. Strauch, Phys. Rev. B **67**, 144304 (2003).
[20]X. Tang and B. Fultz, Phys. Rev. B **84**, 054303 (2011).
[21]K. Esfarjani and H. T. Stokes, Phys. Rev. B **77**, 144112 (2008).
[22]N. Mingo, D. A. Stewart, D. A. Broido, and D. Srivastava, Phys. Rev. B **77**, 033418 (2008).
[23]P. Giannozzi *et al.*, J. Phys.: Condens. Matter **21**, 395502 (2009).
[24]J. M. Soler, E. Artacho, J. D. Gale, A. Garcia, J. Junquera, P. Ordejon, and D. Sanchez-Portal, J. Phys.: Condens. Matter **14**, 2745 (2002).
[25]U. von Barth and R. Car (unpublished); for a brief description of this method, see A. dal Corso, S. Baroni, R. Resta, and S. de Gironcoli, Phys. Rev. B **47**, 3588 (1993).
[26]G. B. Bachelet, D. R. Hamann, and M. Schluter, Phys. Rev. B **26**, 4199 (1982).
[27]J. Tani and H. Kido, Comput. Mater. Sci. **42**, 531 (2008).
[28]S. Ganeshan, S. L. Shang, Y. Wang, and Z.-K. Liu, J. Alloys Compd. **498**, 191 (2010).
[29]S. Duman, H. M. Tütüncü, S. Baci, and G. P. Srivastava, AIP Conf. Proc. **899**, 247 (2007).
[30]P. Boulet, M. J. Verstraete, J.-P. Crocombette, M. Briki, and M.-C. Record, Comput. Mater. Sci. **50**, 847 (2011).
[31]M. T. Hutchings, T. W. D. Farley, M. A. Hackett, W. Hayes, S. Hull, and U. Steigenberger, Solid State Ionics **28–30**, 1208 (1988).
[32]R. J. Kearney, T. G. Worlton, and R. E. Schmunk, J. Phys. Chem. Solids **31**, 1085 (1970).
[33]R. Viennois, P. Jund, C. Colinet, and J.-C. Tedenac, J. Solid State Chem. **193**, 133 (2012).
[34]P. G. Klemens, Proc. R. Soc. London A **208**, 108 (1951).
[35]L. Lindsay, D. A. Broido, and N. Mingo, Phys. Rev. B **83**, 235428 (2011).
[36]L. Lindsay, D. A. Broido, and T. L. Reinecke, Phys. Rev. Lett. **109**, 095901 (2012).
[37]J. J. Martin, J. Phys. Chem. Solids **33**, 1139 (1972).
[38]J. Tani and H. Kido, Physica B **364**, 218 (2005).
[39]M. Yang, L. Zhang, and Q. Shen, J. Wuhan Univ. Technol. Mater. Sci. Ed. **24**, 912 (2009).
[40]M. Akasaka, T. Iida, T. Nemoto, J. Soga, J. Sato, K. Makino, M. Fukano, and Y. Takanashi, J. Cryst. Growth **304**, 196 (2007).
[41]T. Nemoto, M. Akasaka, T. Iida, J. Sato, J. Soga, K. Nishio, T. Takei, and Y. Takanashi, in *25th International Conference on Thermoelectrics: ICT 06* (2006).
[42]H. Y. Chen, N. Savvides, T. Dasgupta, C. Stiewe, and E. Mueller, Phys. Status Solidi A **207**, 2523 (2010).
[43]Z. Tian, J. Garg, K. Esfarjani, T. Shiga, J. Shiomi, and G. Chen, Phys. Rev. B **85**, 184303 (2012).
[44]S. Henry and G. Chen, J. Comput. Theor. Nanosci. **5**, 141 (2008).
[45]J. Garg, N. Bonini, B. Kozinsky, and N. Marzari, Phys. Rev. Lett. **106**, 045901 (2011).
[46]W. Liu and A. Balandin, J. Appl. Phys. **97**, 073210 (2005).
[47]B. C. Daly, H. J. Maris, A. V. Numikko, and M. Kuball, J. Appl. Phys. **92**, 3820 (2002).
[48]A. Khitun, A. Balandin, K. L. Wang, and G. Chen, Physica E **8**, 13 (2000).
[49]J. Zou and A. Balandin, J. Appl. Phys. **89**, 2932 (2001).
[50]E. P. Pokatilov, D. L. Nika, and A. A. Balandin, Phys. Rev. B **72**, 113311 (2005).